(Received 11 February 2024, Accepted 12 April 2024, Scheduled 27 April 2024)

Role of Power Density, Frequency, Direction of Arrival and Polarization of Incident Field on Specific Absorption Rate Distribution inside a Multilayer Fruits Model

Ardhendu Kundu[1, *], Bhaskar Gupta[2], and Amirul I. Mallick[3]

[1] *Institute of Engineering & Management under University of Engineering & Management, Kolkata, West Bengal, India*
[2] *Electronics and Telecommunication Engineering Department, Jadavpur University, Kolkata, West Bengal, India*
[3] *Department of Biological Sciences, Indian Institute of Science Education and Research Kolkata Mohanpur, Nadia, West Bengal, India*

ABSTRACT: Electromagnetic energy is being utilized over multiple frequency bands to sustain high speed wireless communication systems around the globe. As a consequence, living bodies such as humans, animals, plants, and fruits continuously get exposed to electromagnetic radiation. To safeguard human health, a number of diversified international and national electromagnetic regulatory standards have been prescribed across geographical boundaries for limiting electromagnetic radiation — specific absorption rate and reference power density limits have been prescribed by the international organizations to protect humans from immediate thermal effects. However, reference power density limits differ by ten to hundred times across geographical boundaries depending upon the electromagnetic standards in effect. Moreover, prescribed reference power density limit also varies with frequency of irradiation. On the other hand, plants and fruits possess reasonably high permittivity and electrical conductivity that contribute to considerable electromagnetic energy absorption rates inside typical plant and fruit models. In addition, plants and fruits are primarily asymmetric in nature, and therefore direction of arrival and polarization of incident electromagnetic field are two additional factors that significantly influence the amplitude and spatial distribution of specific absorption rate. Therefore, prescribing only the maximum permissible power density limit in far field seems inadequate. To address these issues, specific absorption rates inside a typical multilayer mango fruits model have been estimated at five different frequencies in accordance with four different international and national electromagnetic regulatory standards (with contrasting reference power density limits) — the magnitudes and spatial distributions of specific absorption rates have been quantified and reported at different frequencies as well as for distinct averaging techniques. Moreover, the impact of direction of arrival and polarization of incident electromagnetic field on the magnitude and spatial distribution of specific absorption rate has also been investigated. A total of one hundred and twenty rigorous simulations has been performed, and as a consequence, four hundred and eighty specific absorption rate data points have been analyzed. Wide disagreement in specific absorption rate data is observed due to variations in four factors mentioned above, i.e., reference power density, frequency, direction of arrival, and polarization of incident electromagnetic field. Moreover keeping all the other factors unaltered, specific absorption rate cannot be directly correlated with the reference power density limit primarily due to non-identical and asymmetric structures of bunch of fruits and plants in most practical scenarios. Thus, observations indicate the necessity of adopting globally harmonized electromagnetic regulatory standards and direct adoption of specific absorption rate limit for plants and fruits instead of only the reference power density limits in far field exposure scenario.

1. INTRODUCTION

High speed wireless communication services are prime need of the hour in current global scenario where people need to work from home/remote office location, interact via online meetings; students need to learn using digital classrooms, etc. Thus with the ever increasing demand of high speed wireless telecommunication services and other applications, electromagnetic energy is being extensively utilized over multiple frequency bands. As a consequence, all living objects such as humans, animals, plants, and fruits are being exposed to continuous electromagnetic radiations from different sources. In this connection, a number of international and national electromagnetic regulatory standards are in effect worldwide [1–7] — however, these prescribed standards are quite inconsistent due to the development based upon significantly diversified backgrounds, technical specifications, medical inferences, and objectives to protect life [8, 9]. Some of these standards prescribe the basic specific absorption rate (SAR) limits along with reference power density limits to protect human health from immediate thermal effects; a few others aim at mitigating biological effects of long duration exposure; and the rest are prescribed to ensure additional precautions against yet unknown health effects [1–9]. In fact, power density limits prescribed by these organizations differ by ten to hundred times [8, 9]. In addition, prescribed reference power density limit also varies with frequency of irradiation [1–7]. Therefore, the impact on electro-

* Corresponding author: Ardhendu Kundu (ardhendukundu.1989@gmail.com).

magnetic energy absorption rates in living biological objects due to above noted contrast in reference power density limits should be investigated [8, 9]. Recent articles report SAR, i.e., the rate at which electromagnetic energy is absorbed in biological object while it is exposed to an external incident field increases with frequency of exposure [9–15].

On the other hand, none of these regulatory organizations have considered electromagnetic energy absorption in plants and fruits along with consequent effects while preparing the standards [1–7, 9]. Thus, in actual circumstances, plants and fruits are being exposed to electromagnetic radiation in accordance with regulatory norms prescribed for humans. Moreover, plant and fruit tissues possess reasonably high permittivity and electrical conductivity due to the presence of adequate water and ion substances [16–23]. It should also be noted that the effective dielectric properties of plant and fruit tissues are considerably higher than most human tissues primarily because of higher water content and ion concentration. Therefore, investigating electromagnetic energy absorption rates in terms of SAR inside different prototype plant and fruit phantoms is an absolute necessity as indicated in literature too [9–15]. Moreover in many cases, plant and fruit structures are multilayer and asymmetric in nature [9, 12, 15]; hence, direction of arrival and polarization of incident wave are two potential factors that perhaps can play crucial role in determining magnitude of SAR value along with its spatial distribution. Thus, it should be investigated whether prescribing only the maximum reference power density limits in far field exposure scenario is sufficient, or a basic SAR limit is required for plants and fruits too. In this connection, a multilayer mango fruits model with connected leaf structure has been reported in literature; the same demonstrated the dependence of absorbed electromagnetic energy distribution on direction of arrival and polarization of incident field at two selective frequencies in accordance with the International Commission on Non-Ionizing Radiation Protection (ICNIRP) guidelines [24]. However, the collective impact of different combinations of reference power density limit, frequency of irradiation, direction of arrival, and polarization of incident wave on SAR distributions in the multilayer mango fruits model should be investigated. Hence, this article considerably extends the earlier reported work at three more frequencies and as per four different international and national electromagnetic standards in combination with six different directions of arrival and polarizations of incident electromagnetic field. Total four hundred and eighty SAR data, obtained from hundred and twenty simulations, have been analyzed in this article to replicate different possible far field exposure scenarios.

2. MATERIAL CHARACTERIZATION, MODELING AND SIMULATION

2.1. Dielectric Properties and Material Density Characterization Technique

Dielectric properties of any medium are characterized by its permittivity and electrical conductivity/loss tangent. Permittivity defines the ability of a medium to store energy from an external incident electric field whereas electrical conductivity/loss tangent determines the amount of electromagnetic energy that gets converted to any other form of energy (in particular to heat energy). A number of standard measurement techniques are available for characterizing dielectric properties of materials — however, the choice of suitable technique depends upon the physical state and dimensions of material under test, surface smoothness, electrical conductivity range, frequency of interest, temperature, and required measurement accuracy limit, etc. [25–27]. The open ended coaxial probe technique is a well established noninvasive method for characterizing dielectric properties of biological tissues [22, 23, 26–29]. The lumped equivalent circuit for open ended coaxial probe can be represented by a parallel combination of fringing capacitance from inner to outer conductor via intervening material inside the coaxial structure, fringing capacitance from inner to outer conductor through biological tissue along with radiation conductance that signifies propagation loss through the biological tissue. The detailed analyses of the equivalent lumped circuit for open ended coaxial probe are well established in relevant literature [12, 30–36]. Here, the commercial version, i.e., Agilent Technologies 85070E open ended coaxial dielectric measurement probe has been used along with the Agilent Technologies E5071B ENA series vector network analyzer to characterize dielectric properties of green mango pulp, seed, and leaf samples [9–15, 22–24]. Dielectric properties for the above mentioned samples have been measured over 20 MHz to 8.5 GHz frequency spectrum at 25°C. Dielectric properties characterization setup has been illustrated in Figs. 1(a) and 1(b), whereas the measured dielectric properties of different mango tissue specimens have been plotted in Figs. 1(c) and 1(d), respectively. Dielectric properties have been further summarized in Table 1 at the frequencies of interest along with the measured material densities for mango pulp, seed, leaf, and twig specimens [24].

TABLE 1. Measured parameters of different mango tissues.

Tissue	Pulp		Seed		Leaf & twig	
Density	906.25 kg/m^3		914.89 kg/m^3		833.33 kg/m^3	
Frequency	ε_r	tan δ	ε_r	tan δ	ε_r	tan δ
947.5 MHz	71.72	0.171	67.00	0.148	33.61	0.309
1842.5 MHz	70.59	0.160	65.66	0.152	31.45	0.270
2150 MHz	70.24	0.178	65.32	0.174	31.00	0.270
2350 MHz	70.14	0.182	65.29	0.182	30.67	0.272
2450 MHz	69.88	0.190	65.01	0.192	30.63	0.277

2.2. Prototyping a Typical Bunch of Mango Fruits and SAR Simulation Setup

An indigenous multilayer prototype for a bunch of two mango fruits has been developed in CST MWS 2014, which is reported in recent literature [24, 37]. The prototyped model is composed of mango pulp, seed, twigs, and leaf weighing around 235 g mass along with a volume of 260 cm^3. The complex geometric structure shown in Fig. 2(a) and the low quality factor due to lossy dielectric layers inside the multilayer fruits model have led to the choice of time domain solver for achieving a ro-

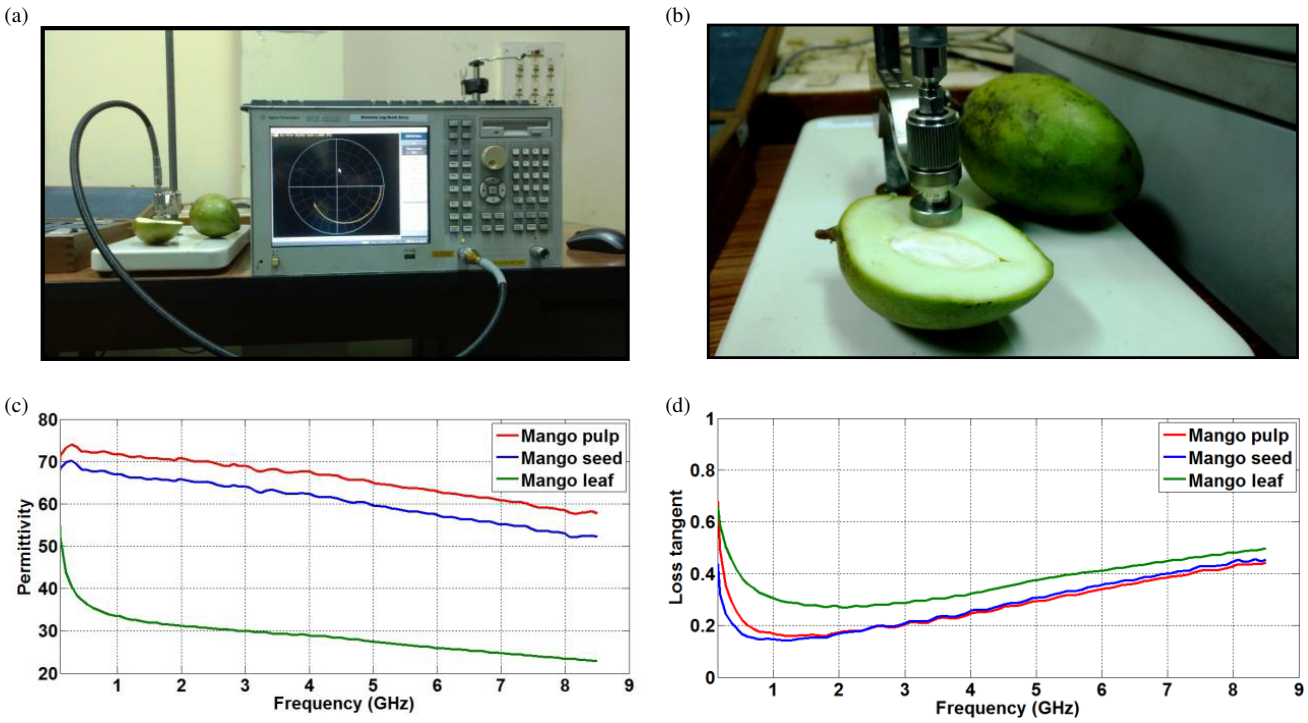

FIGURE 1. (a) Dielectric properties measurement setup for mango pulp, (b) close-up view of dielectric properties measurement setup for mango pulp, (c) measured permittivity for different mango tissues over broadband, and (d) measured loss tangent for different mango tissues over broadband.

bust mesh distribution. This time domain solver is developed based on a computational numerical method called Finite Integration Technique (FIT) — it was first introduced way back in 1977 [38, 39]. The Maxwell's integral equations are discretized and solved using numerical techniques inside the prototyped multilayer fruits model, i.e., the desired solution space. The whole prototyped multilayer mango fruits model is discretized in space with infinitesimal hexahedral meshes of variable size — one wavelength of spatial distance inside the dielectric layers is subdivided into 20 segments. The typical mesh cell count for the above mentioned bunch of mango fruits is observed to be around 6.5 lakh — moreover, the average mass of individual mesh cell is around 0.0015 g. Four perfectly matched layers with 10^{-4} reflection coefficient have been used as electromagnetic absorbing boundaries. Separation between the prototyped bunch of mango fruits structure and the absorbing boundary wall has been set negligible by choosing appropriate boundary conditions — thus, the plane wave can be excited very close to the prototyped structure [9]. Next, the above mentioned bunch of mango fruits has been exposed to linearly polarized plane waves with different combinations of directions of propagation and wave polarizations at five different frequencies (refer to Fig. 2(b)). After satisfying the steady state energy criterion, an inverse transformation precision of -40 dB has been preferred in all the time domain simulations to obtain the frequency domain responses [9, 37]. Maximum local point SAR (MLP SAR), 1 g averaged SAR, 10 g averaged SAR, and whole body averaged SAR (WBA SAR) data have been simulated in accordance with four different international and national electromagnetic standards for different directions of incidence and polarizations of incident field [1–4, 9]. All together, one hundred and twenty electromagnetic simulations have been performed — next, four hundred and eighty SAR data points have been analyzed in subsequent steps. All reported SAR data have been evaluated using the most updated IEEE/IEC 62704-1 SAR averaging protocol [9, 37, 40]. As described in this protocol, once the Maxwell's integral equations have been solved, and electric field strengths on the edges of a grid cell are known, the average electric fields along all three axes are calculated. Next, the effective electric field at the grid centre is obtained and further utilized to calculate point SAR $= \sigma|E|^2/2\rho$. Here, σ is the electrical conductivity of the tissue, E the effective peak electric field strength at the grid centre, and ρ the tissue density. Next, a cubical volume is uniformly expanded along all three axes centering a particular grid cell to achieve the desired SAR averaging mass. In a few cases, this cubical volume can include at most 10 percent background material near the structural boundaries, but the background material mass is not taken into consideration to achieve the averaging mass. Thus, 1 g or 10 g averaged spatial SAR values have been calculated for a particular grid cell — this averaging technique is repeated positioning each valid grid cell at the centre of the averaging cube. Finally, 1 g or 10 g averaged spatial SAR distributions on and inside the prototyped mango fruits model have been obtained using the earlier calculated spatial averaged SAR data of all individual grid cells in the prototyped structure. This is how spatial SAR averaging has been performed in accordance with the IEEE/IEC 62704-1 SAR averaging protocol — more detailed descriptions are available in literature [9, 40].

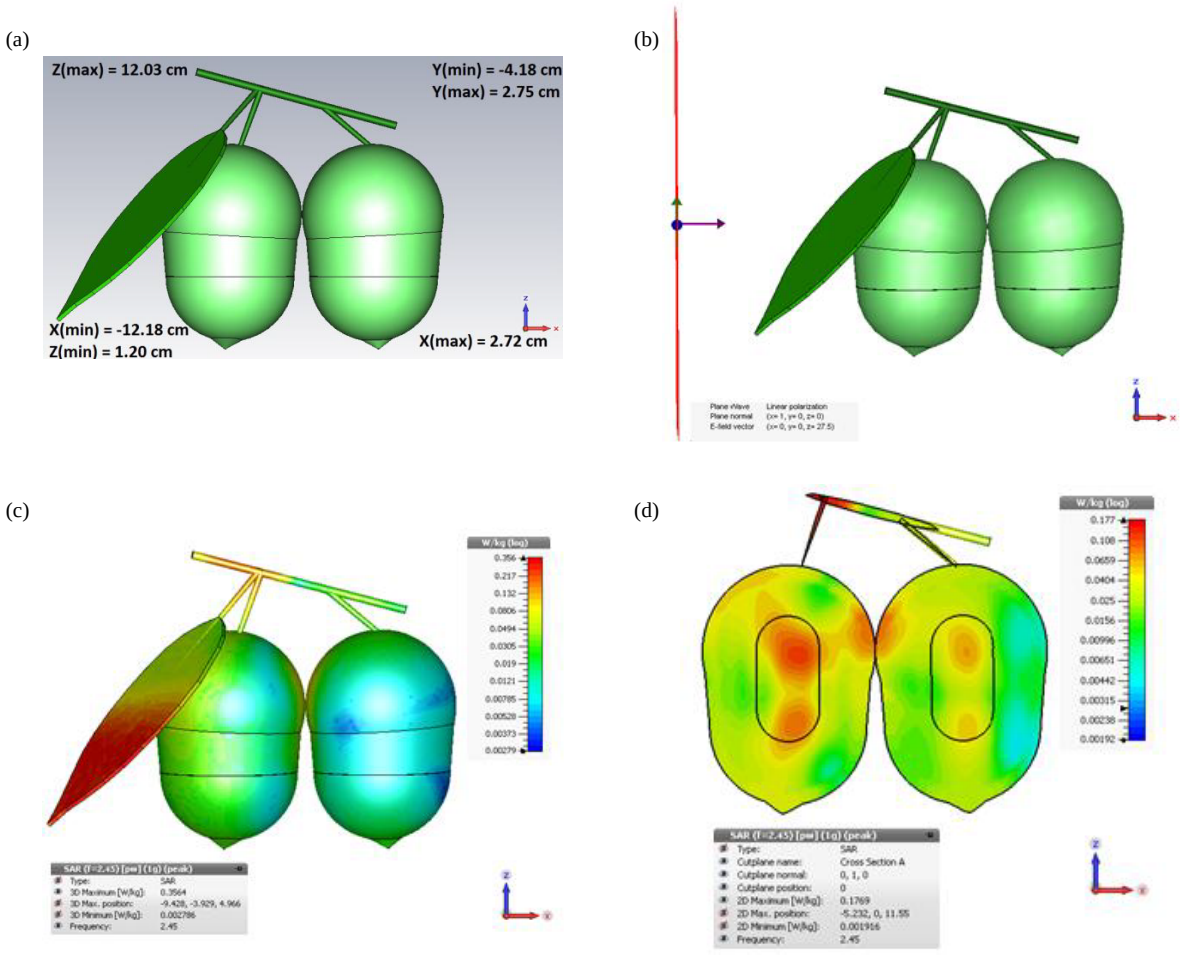

FIGURE 2. (a) Three dimensional perspective of the designed bunch of mango fruits model with marked coordinates, (b) the bunch of mango fruits model is exposed to a linearly polarized plane wave propagating along x axis and electric field along z axis, (c) 1 g SAR distribution on three dimensional surface of the bunch of mango fruits model at 2.45 GHz as per the existing Indian public scenario, (d) 1 g SAR distribution on a two dimensional cut plane of the bunch of mango fruits model at 2.45 GHz as per the existing Indian public scenario.

3. INTERNATIONAL AND NATIONAL ELECTROMAGNETIC EXPOSURE STANDARDS

With the increasing utilization of wireless communication systems, investigations on electromagnetic energy absorption rates and consequent effects in humans along with other living bodies are being conducted worldwide [9–15, 41–66]. However, research studies are being conducted primarily on humans and animals with little emphasis on plants, crops, and fruits [41–58]. It should be noted that the SAR values as well as linked biological effects are expected to differ depending upon field strength even at a particular frequency. Therefore, different international and national electromagnetic standards together with their contrast should be discussed before investigating the SAR distributions in the designed bunch of mango fruits model for different combinations of directions of incidence and wave polarizations.

Significant contrast in the premises, medical backgrounds, technical specifications, and the purposes of different international and national electromagnetic standards is always there. It is because some standards are developed to mitigate immediate thermal effects, a few others aim at minimizing the non-thermal biological consequences over extended duration, and the rest have been prescribed on the basis of precautions against yet unknown effects on humans [8, 9]. However, none of these standards have been prescribed to safeguard plants. Global electromagnetic standards prescribed by the Federal Communications Commission (FCC) and ICNIRP have been adopted worldwide in many countries to counter possible human health risks [1, 2]. However, the reference power density (below 2 GHz) and basic SAR limits prescribed by these two organizations are not in exact agreement. In contrast, recent reported SAR data for different human models along with the possible consequences have raised concerns among the scientists and common public in selected countries [41–61, 67]. In response, some countries like India, Switzerland, etc. have adopted much stricter national regulatory policies [3, 4, 9]. As a consequence, the plane wave equivalent reference power density limits at public zone differ by ten to hundred times across geographical boundaries based on the regulatory standards in effect (refer to Table 2) [8, 9]. It should also be noted that the public exposure policies in Russia, Italy, etc. are very strict like in Switzerland, thus, those electromagnetic policies have not been discussed separately [5–9].

TABLE 2. Overview of different international and national electromagnetic exposure regulatory standards [1–4, 9].

Frequency (MHz)	Reference power density limit (W/m^2)					
	Occupational		Public			
	FCC	ICNIRP	FCC	ICNIRP	India	Swiss
947.5	31.58	23.69	6.32	4.74	0.47	0.047
1842.5	50	46.06	10	9.21	0.92	0.092
2150	50	50	10	10	1	0.1
2350	50	50	10	10	1	0.1
2450	50	50	10	10	1	0.1

TABLE 3. Comparative SAR data at 947.5 MHz for different directions of arrival and polarizations of incident wave.

Frequency 947.5 MHz												
Direction and polarization of incident wave	FCC			ICNIRP			India			Swiss		
	MLP SAR	1g SAR	10g SAR	MLP SAR	1g SAR	10g SAR	MLP SAR	1g SAR	10g SAR	MLP SAR	1g SAR	10g SAR
DoP: y = 1, E-field: z axis	6.97	0.87	0.47	5.22	0.65	0.35	0.52	0.06	0.035	0.05	0.006	0.003
DoP: y = -1, E-field: z axis	7.06	0.87	0.47	5.30	0.65	0.35	0.53	0.06	0.035	0.05	0.006	0.003
DoP: x = 1, E-field: z axis	6.55	1.06	0.61	4.91	0.80	0.46	0.49	0.08	0.046	0.04	0.008	0.004
DoP: x = -1, E-field: z axis	7.34	1.01	0.59	5.51	0.76	0.44	0.55	0.07	0.044	0.05	0.007	0.004
DoP: z = -1, E-field: y axis	1.38	0.41	0.20	1.03	0.31	0.15	0.10	0.03	0.015	0.01	0.003	0.001
DoP: z = -1, E-field: x axis	18.77	3.09	0.93	14.08	2.32	0.70	1.40	0.23	0.070	0.14	0.023	0.007
SAR is in W/Kg												

TABLE 4. Comparative SAR data at 1842.5 MHz for different directions of arrival and polarizations of incident wave.

Frequency 1842.5 MHz												
Direction and polarization of incident wave	FCC			ICNIRP			India			Swiss		
	MLP SAR	1g SAR	10g SAR	MLP SAR	1g SAR	10g SAR	MLP SAR	1g SAR	10g SAR	MLP SAR	1g SAR	10g SAR
DoP: y = 1, E-field: z axis	6.36	1.84	0.56	5.86	1.69	0.51	0.58	0.16	0.051	0.05	0.016	0.005
DoP: y = -1, E-field: z axis	5.95	1.01	0.46	5.48	0.93	0.43	0.54	0.09	0.043	0.05	0.009	0.004
DoP: x = 1, E-field: z axis	22.23	2.19	0.94	20.48	2.02	0.86	2.04	0.20	0.087	0.20	0.020	0.008
DoP: x = -1, E-field: z axis	22.61	1.90	0.83	20.83	1.75	0.77	2.08	0.17	0.077	0.20	0.017	0.007
DoP: z = -1, E-field: y axis	2.39	1.31	0.63	2.20	1.21	0.58	0.22	0.12	0.058	0.02	0.012	0.005
DoP: z = -1, E-field: x axis	16.11	2.30	1.11	14.84	2.12	1.02	1.48	0.21	0.102	0.14	0.021	0.010
SAR is in W/Kg												

TABLE 5. Comparative SAR data at 2150 MHz for different directions of arrival and polarizations of incident wave.

Frequency 2150 MHz												
Direction and polarization of incident wave	FCC			ICNIRP			India			Swiss		
	MLP SAR	1g SAR	10g SAR	MLP SAR	1g SAR	10g SAR	MLP SAR	1g SAR	10g SAR	MLP SAR	1g SAR	10g SAR
DoP: y = 1, E-field: z axis	6.06	2.55	0.72	6.06	2.55	0.72	0.59	0.25	0.072	0.06	0.025	0.007
DoP: y = -1, E-field: z axis	5.20	1.10	0.46	5.20	1.10	0.46	0.51	0.10	0.046	0.05	0.011	0.004
DoP: x = 1, E-field: z axis	20.53	2.77	0.90	20.53	2.77	0.90	2.06	0.27	0.089	0.20	0.027	0.008
DoP: x = -1, E-field: z axis	18.21	1.54	0.61	18.21	1.54	0.61	1.80	0.15	0.061	0.18	0.015	0.006
DoP: z = -1, E-field: y axis	2.40	1.20	0.45	2.40	1.20	0.45	0.240	0.12	0.045	0.02	0.012	0.004
DoP: z = -1, E-field: x axis	16.42	2.39	1.06	16.42	2.39	1.06	1.62	0.23	0.106	0.16	0.023	0.010
SAR is in W/Kg												

4. SAR RESULTS AND ANALYSES

The dependence of SAR magnitude and its distribution inside the typical bunch of mango fruits model on reference power density limit, frequency of irradiation, direction of arrival, and wave polarization has been investigated in this work. However, a prior discussion on the typical SAR distribution on three dimensional external surface and on specific internal cut plane of the bunch of mango fruits model is deemed necessary. Figs. 2(c) and 2(d) illustrate 1 g averaged SAR distributions respectively on three dimensional surface and on specific two di-

TABLE 6. Comparative SAR data at 2350 MHz for different directions of arrival and polarizations of incident wave.

Frequency 2350 MHz												
Direction and polarization of incident wave	FCC			ICNIRP			India			Swiss		
	MLP SAR	1g SAR	10g SAR	MLP SAR	1g SAR	10g SAR	MLP SAR	1g SAR	10g SAR	MLP SAR	1g SAR	10g SAR
DoP: y = 1, E-field: z axis	7.40	3.02	0.81	7.40	3.02	0.81	0.71	0.29	0.080	0.07	0.030	0.008
DoP: y = -1, E-field: z axis	6.31	1.00	0.45	6.31	1.00	0.45	0.61	0.10	0.045	0.06	0.010	0.004
DoP: x = 1, E-field: z axis	21.76	3.24	0.89	21.76	3.24	0.89	2.09	0.31	0.088	0.21	0.032	0.008
DoP: x = -1, E-field: z axis	17.87	1.23	0.49	17.87	1.23	0.49	1.73	0.12	0.050	0.17	0.012	0.004
DoP: z = -1, E-field: y axis	2.98	1.51	0.46	2.98	1.51	0.46	0.29	0.14	0.046	0.02	0.015	0.004
DoP: z = -1, E-field: x axis	14.02	2.61	1.07	14.02	2.61	1.07	1.39	0.25	0.106	0.13	0.026	0.010
SAR is in W/Kg												

TABLE 7. Comparative SAR data at 2450 MHz for different directions of arrival and polarizations of incident wave.

Frequency 2450 MHz												
Direction and polarization of incident wave	FCC			ICNIRP			India			Swiss		
	MLP SAR	1g SAR	10g SAR	MLP SAR	1g SAR	10g SAR	MLP SAR	1g SAR	10g SAR	MLP SAR	1g SAR	10g SAR
DoP: y = 1, E-field: z axis	8.20	3.36	0.87	8.20	3.36	0.87	0.82	0.33	0.087	0.08	0.033	0.008
DoP: y = -1, E-field: z axis	7.81	1.05	0.43	7.81	1.05	0.43	0.78	0.10	0.043	0.07	0.010	0.004
DoP: x = 1, E-field: z axis	24.11	3.56	0.92	24.11	3.56	0.92	2.41	0.35	0.092	0.24	0.035	0.009
DoP: x = -1, E-field: z axis	17.30	1.09	0.44	17.30	1.09	0.44	1.73	0.10	0.044	0.17	0.011	0.004
DoP: z = -1, E-field: y axis	2.97	1.68	0.45	2.97	1.68	0.45	0.29	0.16	0.045	0.03	0.016	0.004
DoP: z = -1, E-field: x axis	15.76	2.69	1.08	15.76	2.69	1.08	1.57	0.26	0.10	0.15	0.026	0.010
SAR is in W/Kg												

mensional cut plane of prototyped bunch of mango fruits model at 2.45 GHz as per the existing Indian public exposure scenario. The SAR distributions are consequences of linearly polarized plane wave irradiation with the direction of propagation along the x axis and electric field variation along the z axis. It is observed that the SAR value increases on and around regions with higher curvature or near dielectric boundaries, because the magnitude of charge accumulation tends to increase on surface region with greater curvature as obtained by solving Poisson's equation on and around the surface of an arbitrary shaped structure [68]. Local electric field distribution also follows a similar pattern due to such nonuniform charge distribution, i.e., electric field strength at regions with greater charge density is greater in magnitude [69]. This phenomenon of concentrated electric field near sharp edges is not only true for conducting bodies but also applies to dielectric objects with reasonably high electrical conductivity/loss tangent [70]. Analysis of the scattering problem, i.e., scattering of incident electromagnetic field due to a lossy dielectric body, generally leads to an electric field distribution or equivalent induced surface current density that prefers to be in close vicinity of sharp edges — magnitude of surface current distribution is more in close vicinity of greater surface curvature. Hence, increased electromagnetic energy absorption rate near sharp geometries of prototype bunch of mangoes can cause localized effects, and it should not be averaged over nearby masses with less electromagnetic energy absorption rates [9].

Next, let's consider the effect of reference power density limit which is regulated by the electromagnetic standards in effect; SAR data have been estimated for the prototyped bunch of mango fruits model over five different frequencies in accordance with the FCC and ICNIRP prescribed international public exposure standards [1, 2]. In addition, SAR data have also been simulated as per the existing Indian and Swiss national electromagnetic regulatory policies (refer to Table 2) [3, 4, 9]. It is noted that for a particular combination of frequency, direction of incidence, and wave polarization, SAR values for the bunch of mango fruits model are widely contrasting in nature depending upon the reference power density limit (i.e., the regulatory standards) in effect [9]. Data presented in Table 3 to Table 7 illustrate that SAR value increases proportionately with the prescribed reference power density limit irrespective of frequency of irradiation. Thus, be it MLP SAR, 1 g averaged SAR or 10 g averaged SAR, it is always maximum corresponding to public exposure in accordance with the FCC standards; however, SAR data are also quite high as per the ICNIRP norms for public exposure (below 2000 MHz) and at par with the FCC standards beyond 2000 MHz. Simulated SAR data in accordance with the existing Indian scenario are moderate at $1/10^{\text{th}}$ levels of the ICNIRP scenario [3, 9]. The most stringent SAR values are noted as per the Swiss public exposure standards at $1/100^{\text{th}}$ levels of the ICNIRP scenario [4, 9]. Both reference power density and SAR value are dependent upon second degree of electric field strength magnitude at their respective points of measurement [1–4, 9–15]; hence, contrast in SAR value for the designed bunch of mango fruits model exactly follows contrasting nature of the reference power density limits as per the above mentioned international and national electromagnetic regulatory standards [1–4, 9].

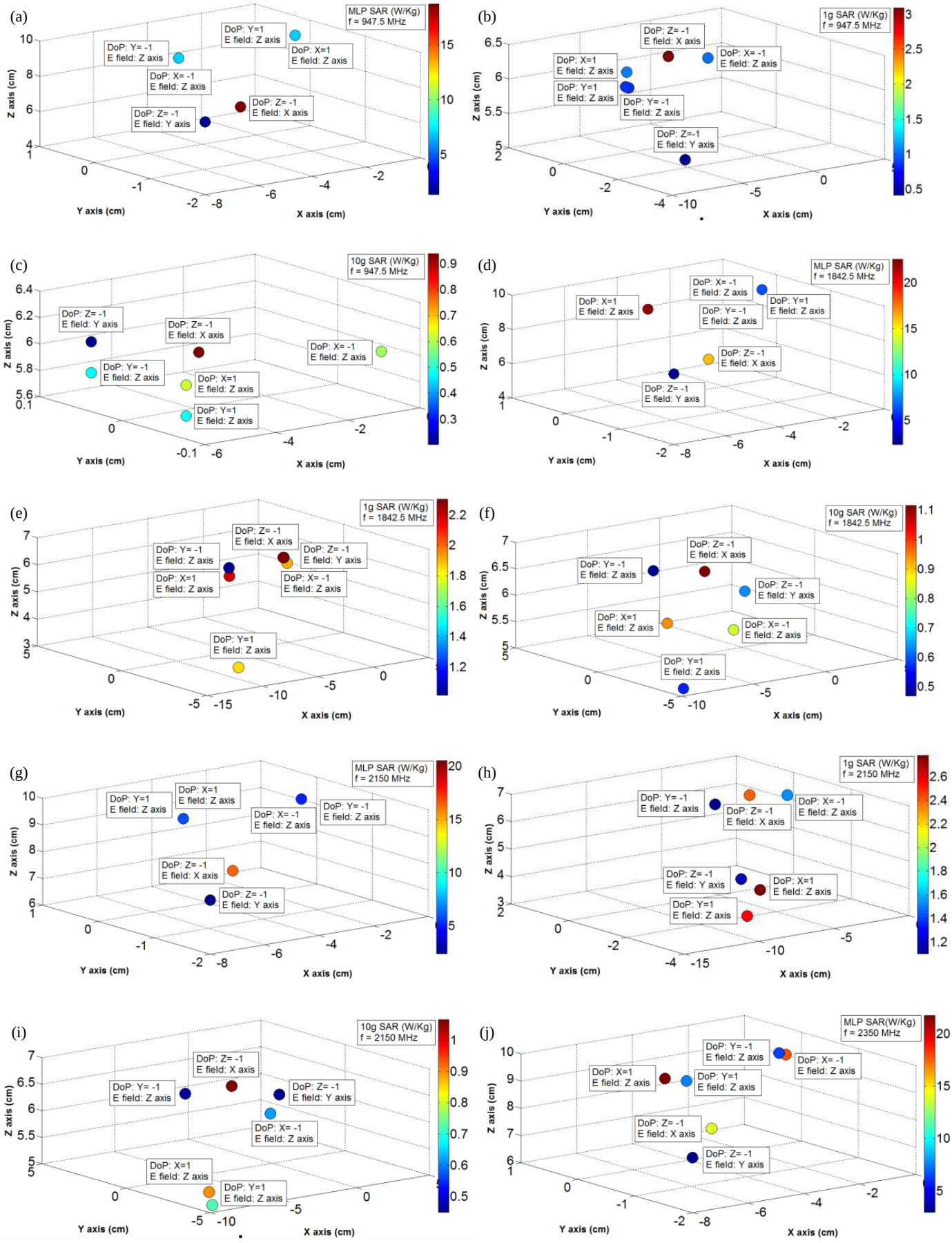
(a)
MLP SAR (W/Kg)
f = 947.5 MHz
DoP: Y= -1
E field: Z axis
DoP: Y=1
E field: Z axis
DoP: X=1
E field: Z axis
DoP: X= -1
E field: Z axis
DoP: Z= -1
E field: Y axis
DoP: Z= -1
E field: X axis
Z axis (cm)
Y axis (cm)
X axis (cm)
(b)
1g SAR (W/Kg)
f = 947.5 MHz
DoP: Z= -1
E field: X axis
DoP: X=1
E field: Z axis
DoP: X= -1
E field: Z axis
DoP: Y=1
E field: Z axis
DoP: Y= -1
E field: Z axis
DoP: Z=-1
E field: Y axis
Z axis (cm)
Y axis (cm)
X axis (cm)
(c)
10g SAR (W/Kg)
f = 947.5 MHz
DoP: Z= -1
E field: Y axis
DoP: Z= -1
E field: X axis
DoP: X= -1
E field: Z axis
DoP: Y= -1
E field: Z axis
DoP: X=1
E field: Z axis
DoP: Y=1
E field: Z axis
Z axis (cm)
Y axis (cm)
X axis (cm)
(d)
MLP SAR (W/Kg)
f = 1842.5 MHz
DoP: X= -1
E field: Z axis
DoP: X=1
E field: Z axis
DoP: Y= -1
E field: Z axis
DoP: Y=1
E field: Z axis
DoP: Z= -1
E field: X axis
DoP: Z= -1
E field: Y axis
Z axis (cm)
Y axis (cm)
X axis (cm)
(e)
1g SAR (W/Kg)
f = 1842.5 MHz
DoP: Z= -1
E field: X axis
DoP: Y= -1
E field: Z axis
DoP: Z= -1
E field: Y axis
DoP: X=1
E field: Z axis
DoP: X= -1
E field: Z axis
DoP: Y=1
E field: Z axis
Z axis (cm)
Y axis (cm)
X axis (cm)
(f)
10g SAR (W/Kg)
f = 1842.5 MHz
DoP: Z= -1
E field: X axis
DoP: Y= -1
E field: Z axis
DoP: Z= -1
E field: Y axis
DoP: X=1
E field: Z axis
DoP: X= -1
E field: Z axis
DoP: Y=1
E field: Z axis
Z axis (cm)
Y axis (cm)
X axis (cm)
(g)
MLP SAR (W/Kg)
f = 2150 MHz
DoP: Y=1
E field: Z axis
DoP: X=1
E field: Z axis
DoP: X= -1
E field: Z axis
DoP: Y= -1
E field: Z axis
DoP: Z= -1
E field: X axis
DoP: Z= -1
E field: Y axis
Z axis (cm)
Y axis (cm)
X axis (cm)
(h)
1g SAR (W/Kg)
f = 2150 MHz
DoP: Y= -1
E field: Z axis
DoP: Z= -1
E field: X axis
DoP: X= -1
E field: Z axis
DoP: Z= -1
E field: Y axis
DoP: X=1
E field: Z axis
DoP: Y=1
E field: Z axis
Z axis (cm)
Y axis (cm)
X axis (cm)
(i)
10g SAR (W/Kg)
f = 2150 MHz
DoP: Z= -1
E field: X axis
DoP: Y= -1
E field: Z axis
DoP: Z= -1
E field: Y axis
DoP: X= -1
E field: Z axis
DoP: X=1
E field: Z axis
DoP: Y=1
E field: Z axis
Z axis (cm)
Y axis (cm)
X axis (cm)
(j)
MLP SAR(W/Kg)
f = 2350 MHz
DoP: Y= -1
E field: Z axis
DoP: X=1
E field: Z axis
DoP: X= -1
E field: Z axis
DoP: Y=1
E field: Z axis
DoP: Z= -1
E field: X axis
DoP: Z= -1
E field: Y axis
Z axis (cm)
Y axis (cm)
X axis (cm)

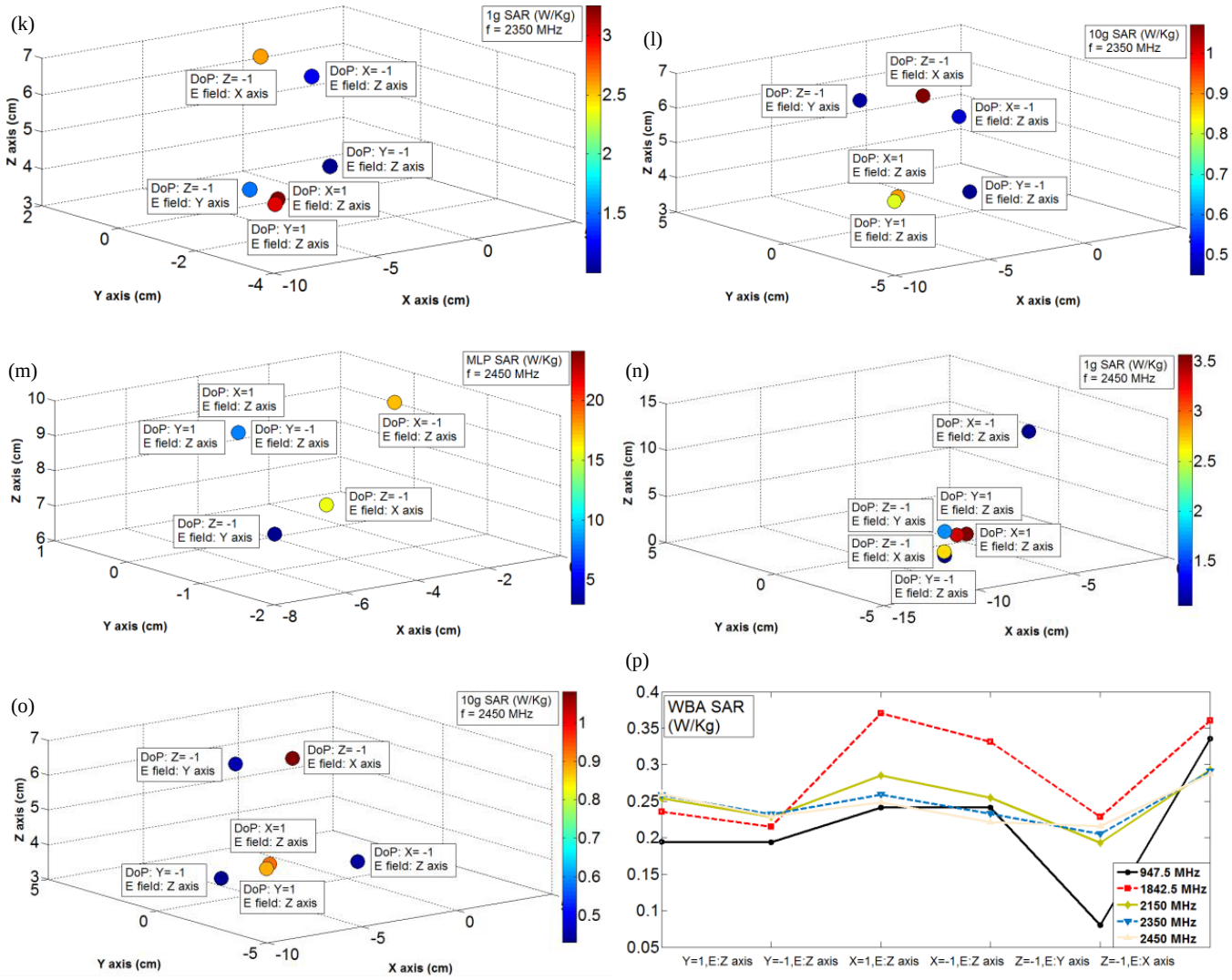

FIGURE 3. SAR data as per the FCC public electromagnetic standards (a) to (c) MLP SAR, 1 g averaged, and 10 g averaged SAR distribution at 947.5 MHz due to variations in direction of arrival and polarization; (d) to (f) MLP SAR, 1 g averaged, and 10 g averaged SAR distribution at 1842.5 MHz due to variations in direction of arrival and polarization; (g) to (i) MLP SAR, 1 g averaged, and 10 g averaged SAR distribution at 2150 MHz due to variations in direction of arrival and polarization; (j) to (l) MLP SAR, 1 g averaged, and 10 g averaged SAR distribution at 2350 MHz due to variations in direction of arrival and polarization; (m) to (o) MLP SAR, 1 g averaged, and 10 g averaged SAR distribution at 2450 MHz due to variations in direction of arrival and polarization; (p) WBA SAR data over all five frequencies due to variations in direction of arrival and polarization.

TABLE 8. Typical Max-to-Min SAR ratio for different combinations of direction of arrival and polarization of incident wave.

Frequency (MHz)	Typical Max/Min SAR ratio for different combinations of direction of arrival and polarization of incident field			
	MLP SAR	1 g SAR	10 g SAR	WBA SAR
947.5	13.66	7.48	4.66	4.16
1842.5	9.46	2.27	2.37	1.79
2150	8.55	2.51	2.35	1.52
2350	7.30	3.24	2.37	1.45
2450	8.11	3.39	2.51	1.32

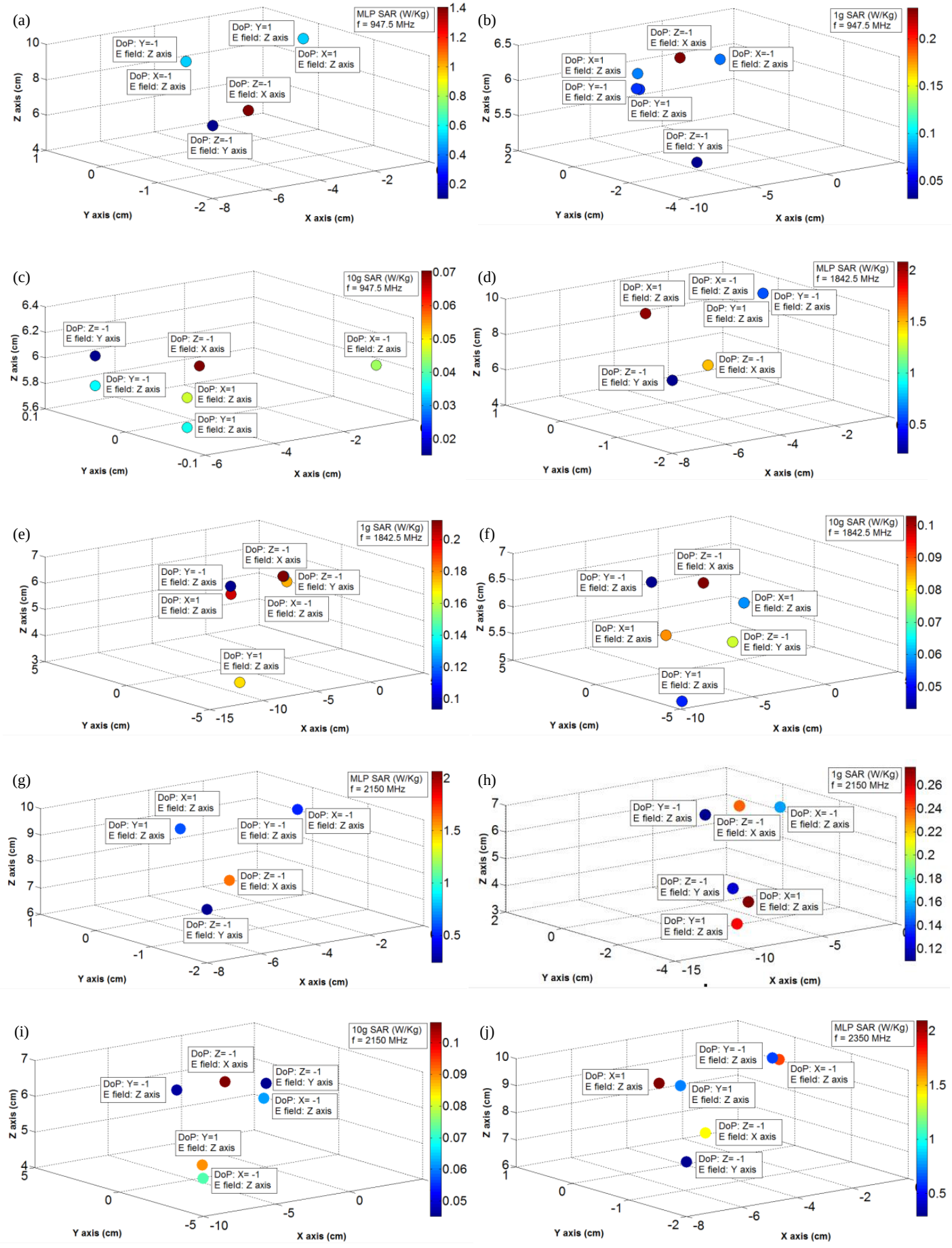
(a)
MLP SAR (W/Kg)
f = 947.5 MHz
DoP: Y=1
E field: Z axis
DoP: Y=-1
E field: Z axis
DoP: X=1
E field: Z axis
DoP: X=-1
E field: Z axis
DoP: Z=-1
E field: X axis
DoP: Z=-1
E field: Y axis
Z axis (cm)
Y axis (cm)
X axis (cm)
(b)
1g SAR (W/Kg)
f = 947.5 MHz
DoP: Z=-1
E field: X axis
DoP: X=1
E field: Z axis
DoP: X=-1
E field: Z axis
DoP: Y=-1
E field: Z axis
DoP: Y=1
E field: Z axis
DoP: Z=-1
E field: Y axis
Z axis (cm)
Y axis (cm)
X axis (cm)
(c)
10g SAR (W/Kg)
f = 947.5 MHz
DoP: Z= -1
E field: Y axis
DoP: Z= -1
E field: X axis
DoP: X= -1
E field: Z axis
DoP: Y= -1
E field: Z axis
DoP: X=1
E field: Z axis
DoP: Y=1
E field: Z axis
Z axis (cm)
Y axis (cm)
X axis (cm)
(d)
MLP SAR (W/Kg)
f = 1842.5 MHz
DoP: X=1
E field: Z axis
DoP: X= -1
E field: Z axis
DoP: Y= -1
E field: Z axis
DoP: Y=1
E field: Z axis
DoP: Z= -1
E field: Y axis
DoP: Z= -1
E field: X axis
Z axis (cm)
Y axis (cm)
X axis (cm)
(e)
1g SAR (W/Kg)
f = 1842.5 MHz
DoP: Z= -1
E field: X axis
DoP: Y= -1
E field: Z axis
DoP: Z= -1
E field: Y axis
DoP: X=1
E field: Z axis
DoP: X= -1
E field: Z axis
DoP: Y=1
E field: Z axis
Z axis (cm)
Y axis (cm)
X axis (cm)
(f)
10g SAR (W/Kg)
f = 1842.5 MHz
DoP: Z= -1
E field: X axis
DoP: Y= -1
E field: Z axis
DoP: X=1
E field: Z axis
DoP: X=1
E field: Z axis
DoP: Z= -1
E field: Y axis
DoP: Y=1
E field: Z axis
Z axis (cm)
Y axis (cm)
X axis (cm)
(g)
MLP SAR (W/Kg)
f = 2150 MHz
DoP: X=1
E field: Z axis
DoP: Y=1
E field: Z axis
DoP: Y= -1
E field: Z axis
DoP: X= -1
E field: Z axis
DoP: Z= -1
E field: X axis
DoP: Z= -1
E field: Y axis
Z axis (cm)
Y axis (cm)
X axis (cm)
(h)
1g SAR (W/Kg)
f = 2150 MHz
DoP: Y= -1
E field: Z axis
DoP: Z= -1
E field: X axis
DoP: X= -1
E field: Z axis
DoP: Z= -1
E field: Y axis
DoP: X=1
E field: Z axis
DoP: Y=1
E field: Z axis
Z axis (cm)
Y axis (cm)
X axis (cm)
(i)
10g SAR (W/Kg)
f = 2150 MHz
DoP: Z= -1
E field: X axis
DoP: Y= -1
E field: Z axis
DoP: Z= -1
E field: Y axis
DoP: X= -1
E field: Z axis
DoP: Y=1
E field: Z axis
DoP: X= -1
E field: Z axis
Z axis (cm)
Y axis (cm)
X axis (cm)
(j)
MLP SAR (W/Kg)
f = 2350 MHz
DoP: Y= -1
E field: Z axis
DoP: X=1
E field: Z axis
DoP: X= -1
E field: Z axis
DoP: Y=1
E field: Z axis
DoP: Z= -1
E field: X axis
DoP: Z= -1
E field: Y axis
Z axis (cm)
Y axis (cm)
X axis (cm)

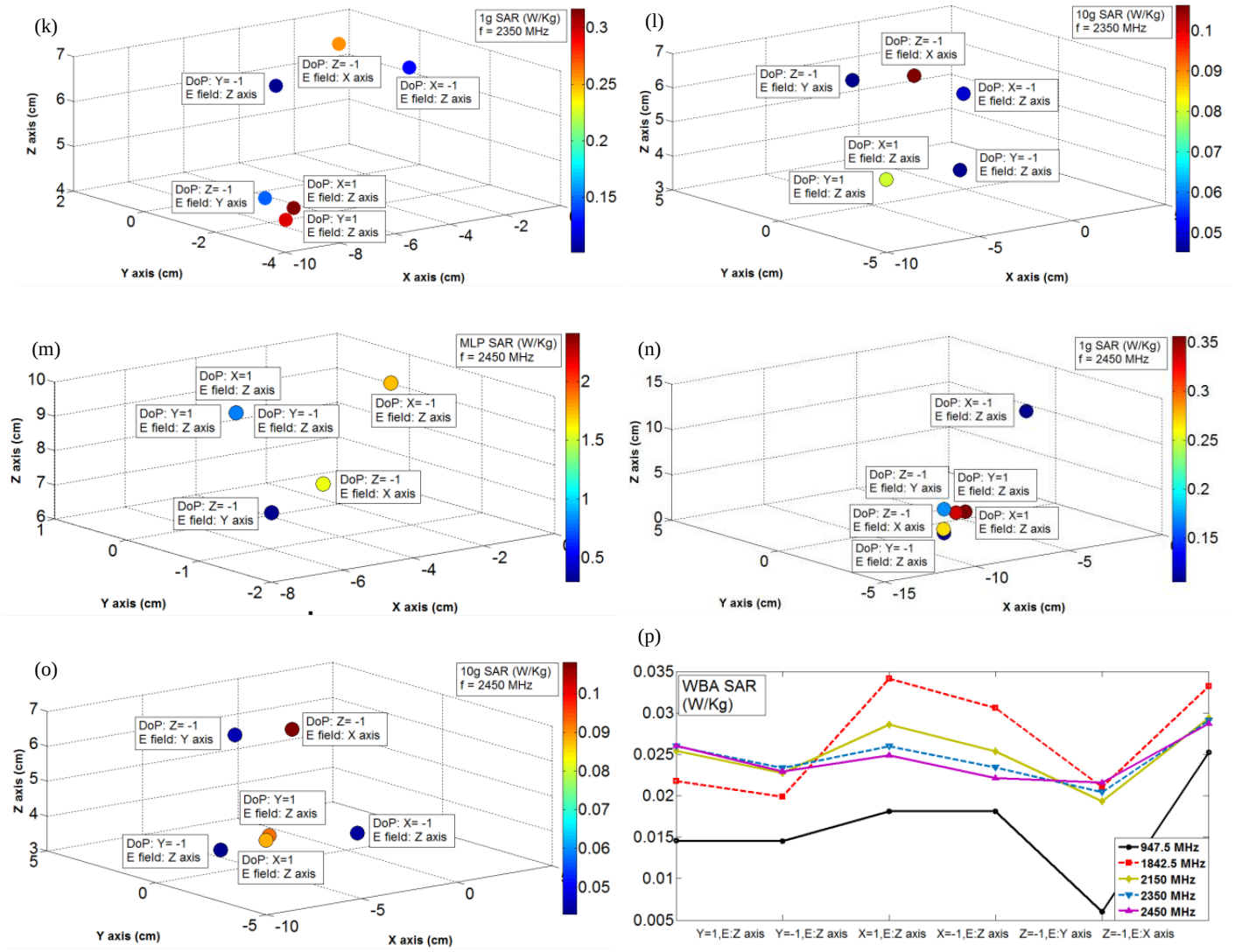

FIGURE 4. SAR data as per the existing Indian public electromagnetic standards (a) to (c) MLP SAR, 1 g averaged, and 10 g averaged SAR distribution at 947.5 MHz due to variations in direction of arrival and polarization; (d) to (f) MLP SAR, 1 g averaged, and 10 g averaged SAR distribution at 1842.5 MHz due to variations in direction of arrival and polarization; (g) to (i) MLP SAR, 1 g averaged, and 10 g averaged SAR distribution at 2150 MHz due to variations in direction of arrival and polarization; (j) to (l) MLP SAR, 1 g averaged, and 10 g averaged SAR distribution at 2350 MHz due to variations in direction of arrival and polarization; (m) to (o) MLP SAR, 1 g averaged, and 10 g averaged SAR distribution at 2450 MHz due to variations in direction of arrival and polarization; (p) WBA SAR data over all five frequencies due to variations in direction of arrival and polarization.

Frequency of irradiation is the second factor that significantly contributes to the SAR magnitude variation along with its distribution in the prototyped bunch of mango fruits model. Keeping all other factors unchanged, SAR magnitude in general varies with the frequency of irradiation as noted in Table 3 to Table 7 [9–15]. Moreover, the spatial SAR distribution along with the position of maximum SAR shifts inside the prototyped bunch of mango fruits model with frequency of irradiation, as illustrated in Figs. 3(a) to 3(p), and Figs. 4(a) to 4(p). The realized wavelength inside biological tissue layers decreases with the increase in frequency of irradiation; as a consequence, more peak formations occur inside the bunch of mango fruits model. Moreover, the maximum permissible reference power density limit increases with frequency of irradiation up to either 1500 MHz or 2000 MHz depending upon the guidelines in effect [1–4]; both these factors influence resultant SAR value [9–15, 24]. As a consequence, 1 g and 10 g averaged SAR values considerably increase from 947.5 MHz to 1842.5 MHz (as seen in Table 3 to Table 4) and thereafter vary at a lower rate with frequency of irradiation.

The magnitude of electromagnetic energy absorption rate and its distribution not only depend upon the reference power density limit and frequency of irradiation — rather, the direction of arrival and polarization of incident wave are also two crucial factors in determining SAR value and its distribution [24]. It is because plant and fruit structures are mostly asymmetric in nature. Observations in Figs. 3(a) to 3(p), Figs. 4(a) to 4(p), and Tables 3–8 indicate that the magnitudes

of MLP SAR, 1 g averaged SAR, 10 g averaged SAR, and their distributions significantly differ due to six different combinations of direction of arrival and polarization of incident wave. The respective maximum variations in MLP SAR, 1 g averaged SAR, 10 g averaged SAR, and WBA SAR are 9.46 times, 2.27 times, 2.37 times, and 1.79 times at 1842.5 MHz due to alterations in direction of arrival and incident wave polarization. Similar variations in electromagnetic energy absorption rate due to different combinations of direction of arrival and polarization of incident wave are observed at all the other frequencies as well (refer to Table 8). A similar trend, indicating the dependence of electromagnetic energy absorption rate on the direction of arrival and wave polarization, has also been reported at selected frequencies in a recent article [24].

The reported data in Table 8 strongly indicate that limiting the reference power density level or the equivalent electric field strength is inadequate to correlate with SAR value and ensure safety of plants, crops, and fruits in far field region because electromagnetic energy absorption rate in asymmetric bunch of mango fruits model is largely dependent upon the direction of arrival and polarization of incident wave. Hence, direct adoption of basic SAR limit for all living bodies including plants, crops, and fruits is more logical even in far field.

5. DISCUSSION

The strength of this investigation lies in the fact that the impact of wide variation in prescribed power density, frequency of exposure, direction of arrival, and polarization of incident wave on spatial SAR distribution inside the typical multilayer mango fruits model has been exclusively demonstrated. Spatial SAR distribution, at the interface of distinct tissue layers, i.e., mango pulp and mango seed, has been illustrated in this article (refer to Fig. 2(d)) — the impedance mismatch at the dielectric tissue layer interface plays a fundamental role. Furthermore, reported fold change in SAR data due to contrast in different international and national reference power density levels is generic and therefore applies to all living biological bodies [1–8]. Simulated SAR data can be a good reference point for validation through practical measurements. Further work is in progress on mango tissue equivalent phantom liquid preparation for practical SAR measurement [71]. However, custom made phantom shell preparation for the designed mango fruits model is challenging — the leaf structure is thin, and field perturbation with probe can affect measured data. Dielectric properties of mango tissues are dependent on fruit maturity level — thus, sample-to-sample variation in measured dielectric properties will also be reflected in simulated SAR results. Cumulative measurement uncertainties have been attempted to minimize by choosing appropriate fruit specimens and sensibly fixing instrument setup [72]. This work establishes the fact that plants and fruits are capable of absorbing significant amount of incident electromagnetic radiation in global exposure scenarios [1–7]. This observation is in line with relevant articles published in recent times [9–15, 24, 72, 73]. Hence, global policymakers should promote further research on subsequent biological effects at plant physiological as well as molecular levels and revise existing electromagnetic exposure policies based on the findings [62–66].

6. CONCLUSION

All reported SAR data have been estimated for public exposure in accordance with different international and national electromagnetic standards (prescribed for humans). However, it must be noted that the reference power density limits are much liberal in the case of occupational exposure scenario; as a consequence, estimated SAR values would increase five times or so for such exposure scenario. Furthermore, SAR values are additive in nature over multiple frequency bands of irradiation; hence, restriction should also be imposed to limit the cumulative SAR value instead of SAR estimated for a single frequency of irradiation.

Electromagnetic energy absorption rate inside the prototyped bunch of mango fruits model varies considerably depending upon each of these factors — i.e., reference power density, frequency, direction of arrival, and polarization of incident wave. Proportionate disagreement in SAR magnitude due to discrepancy in reference power density limit as per the different international and national guidelines indicates the need of uniform regulatory guidelines worldwide. In addition, magnitude as well as spatial distribution of SAR varies significantly with the frequency of irradiation. In general, SAR magnitude increases with the frequency of irradiation because of enhanced reference power density limits (up to either 1500 MHz or 2000 MHz depending upon the guidelines in effect) and increased number of peak formations due to reduced wavelength in biological tissues. Plant and fruit structures are reasonably asymmetric in nature — as a consequence, magnitude and spatial distribution of SAR inside the bunch of mango fruits model crucially vary with direction of arrival and polarization of incident wave. The ratios of maximum SAR magnitude to minimum SAR magnitude at different frequencies are quite significant, as reported in Table 8. In addition, significant variations in spatial SAR distribution due to different directions of arrival and polarizations of incident wave have also been reported. Hence, uniform electromagnetic regulatory standards should be adopted worldwide to ensure the safety of plants, fruits, and crops in addition to humans. Furthermore, direct adoption of maximum allowable SAR limits is also recommended for plant and fruit structures as those are quite asymmetric in nature.

ACKNOWLEDGEMENT

Authors would like to thank School of Nuclear Studies and Application, Jadavpur University for providing the Agilent Technologies 85070E open ended coaxial probe kit to facilitate dielectric properties measurement. In addition, authors also acknowledge Rashtriya Uchchatar Shiksha Abhiyan (RUSA) 2.0 scheme, Ministry of Human Resource and Development, Govt. of India for supporting the research work.

REFERENCES

[1] Means, D. L. and K. W. Chan, "Evaluating compliance with FCC guidelines for human exposure to radiofrequency electromag-

netic fields," *FCC OET Bulletin*, Vol. 65, No. 10, 1–57, Washington D.C., 1997.

[2] International Commission on Non-Ionizing Radiation Protection (ICNIRP), "Guidelines for limiting exposure to electromagnetic fields (100 kHz to 300 GHz)," *Health Physics*, Vol. 118, No. 5, 483–524, 2020.

[3] Department of Telecommunications (DoT), Mobile Communication — Radio Waves & Safety, 1–15, India, 2012.

[4] Swiss Agency for the Environment, Forests and Landscape (SAEFL), Electrosmog in the Environment, 1–56, Switzerland, 2005.

[5] Ministry of Health of the Russian Federation, SanPiN 2.1.8/2.2.4.1190-03: Arrangement and operation of land mobile radiocommunication facilities — Hygienic requirements, 1–17, Russia, 2003.

[6] The president of the council of ministers (Italy), Establishment of exposure limits, attention values, and quality goals to protect the population against electric, magnetic, and electromagnetic field generated at frequencies between 100 kHz and 300 GHz (unofficial translation by P. Vecchia), 1–6, Italy, 2003.

[7] Vecchia, P., "Radiofrequency fields: Bases for exposure limits," in *2 European IRPA Congress on Radiation Protection — Radiation Protection: From Knowledge to Action*, 1–19, Paris, 2006.

[8] Foster, K. R., "Exposure limits for radiofrequency energy: Three models," in *Proceedings of the Eastern European Regional EMF Meeting and Workshop (Criteria for EMF Standards Harmonization)*, 1–6, Varna, Bulgaria, 2001.

[9] Kundu, A., B. Gupta, and A. I. Mallick, "Contrast in specific absorption rate for a typical plant model due to discrepancy among global and national electromagnetic standards," *Progress In Electromagnetics Research M*, Vol. 99, 139–152, 2021.

[10] Kundu, A. and B. Gupta, "Comparative SAR analysis of some Indian fruits as per the revised RF exposure guideline," *IETE Journal of Research*, Vol. 60, No. 4, 296–302, 2014.

[11] Kundu, A., *RF Energy Absorption in Plant Parts due to Cell Tower Radiation*, 1–220, LAP Lambert Academic Publishing, Germany, 2015.

[12] Kundu, A., B. Gupta, and A. I. Mallick, "Specific absorption rate evaluation in a typical multilayer fruit: Coconut with twig due to electromagnetic radiation as per Indian standards," *Microwave Review (Mikrotalasana Revija)*, Vol. 23, No. 2, 24–32, 2017.

[13] Kundu, A., "Specific absorption rate evaluation in apple exposed to RF radiation from GSM mobile towers," in *2013 IEEE Applied Electromagnetics Conference (AEMC)*, 1–2, Bhubaneswar, India, 2013.

[14] Kundu, A. and B. Gupta, "Specific absorption rate evaluation of apple as per FCC RF exposure guideline," in *Recent Development in Electrical, Electronics & Engineering Physics (RDE3P-2013)*, 152–156, Kolkata, India, 2013.

[15] Kundu, A., B. Gupta, and A. I. Mallick, "SAR analysis in a typical bunch of grapes exposed to radio frequency radiation in Indian scenario," in *2016 International Conference on Microelectronics, Computing and Communications (MicroCom)*, 1–5, Durgapur, India, 2016.

[16] Nelson, S. O., "Measuring dielectric properties of fresh fruits and vegetables," in *IEEE Antennas and Propagation Society International Symposium. Digest. Held in conjunction with: USNC/CNC/URSI North American Radio Sci. Meeting (Cat. No. 03CH37450)*, Vol. 4, 46–49, 2003.

[17] Nelson, S. O., "Dielectric spectroscopy of fresh fruits and vegetables," in *2005 IEEE Instrumentation and Measurement Technology Conference (IMTC 2005)*, Vol. 1, 360–364, 2005.

[18] Nelson, S. O., S. Trabelsi, and S. J. Kays, "Correlating dielectric properties of melons with quality," in *2006 IEEE Antennas and Propagation Society International Symposium*, 4849–4852, 2006.

[19] Guo, W.-C., S. O. Nelson, S. Trabelsi, and S. J. Kays, "10–1800-MHz dielectric properties of fresh apples during storage," *Journal of Food Engineering*, Vol. 83, No. 4, 562–569, 2007.

[20] Nelson, S. O., "Dielectric properties of agricultural products and some applications," *Research in Agricultural Engineering*, Vol. 54, No. 2, 104–112, 2008.

[21] Nelson, S. O. and S. Trabelsi, "Dielectric spectroscopy measurements on fruit, meat, and grain," *Transactions of the ASABE, American Society of Agricultural and Biological Engineers*, Vol. 51, No. 5, 1829–1834, 2008.

[22] Kundu, A. and B. Gupta, "Broadband dielectric properties measurement of some vegetables and fruits using open ended coaxial probe technique," in *Proceedings of the 2014 International Conference on Control, Instrumentation, Energy and Communication (CIEC)*, 480–484, Kolkata, India, 2014.

[23] Kundu, A., K. Patra, and B. Gupta, "Broadband dielectric properties evaluation of catharanthus roseus leaf, flower and stem using open ended coaxial probe technique," *Journal of Physical Science*, Vol. 18, 62–69, 2014.

[24] Kundu, A., B. Gupta, and A. I. Mallick, "Dependence of electromagnetic energy distribution inside a typical multilayer fruit model on direction of arrival and polarization of incident field," in *2019 IEEE Radio and Antenna Days of the Indian Ocean (RADIO)*, 1–2, Reunion, France, 2019.

[25] Venkatesh, M. S. and G. S. V. Raghavan, "An overview of dielectric properties measuring techniques," *Canadian Biosystems Engineering*, Vol. 47, No. 7, 15–30, 2005.

[26] Gregory, A. P. and R. N. Clarke, "A review of RF and microwave techniques for dielectric measurements on polar liquids," *IEEE Transactions on Dielectrics and Electrical Insulation*, Vol. 13, No. 4, 727–743, 2006.

[27] Jha, S. N., K. Narsaiah, A. L. Basediya, R. Sharma, P. Jaiswal, R. Kumar, and R. Bhardwaj, "Measurement techniques and application of electrical properties for nondestructive quality evaluation of foods — A review," *Journal of Food Science and Technology*, Vol. 48, No. 4, 387–411, 2011.

[28] Stuchly, M. A., T. W. Athey, G. M. Samaras, and G. E. Taylor, "Measurement of radio frequency permittivity of biological tissues with an open-ended coaxial line: Part II — Experimental results," *IEEE Transactions on Microwave Theory and Techniques*, Vol. 30, No. 1, 87–92, 1982.

[29] Xu, D., L. Liu, and Z. Jiang, "Measurement of the dielectric properties of biological substances using an improved open-ended coaxial line resonator method," *IEEE Transactions on Microwave Theory and Techniques*, Vol. 35, No. 12, 1424–1428, 1987.

[30] Deschamps, G., "Impedance of an antenna in a conducting medium," *IRE Transactions on Antennas and Propagation*, Vol. 10, No. 5, 648–650, 1962.

[31] Stuchly, M. A. and S. S. Stuchly, "Coaxial line reflection methods for measuring dielectric properties of biological substances at radio and microwave frequencies — A review," *IEEE Transactions on Instrumentation and Measurement*, Vol. 29, No. 3, 176–183, 1980.

[32] Athey, T. W., M. A. Stuchly, and S. S. Stuchly, "Measurement of radio frequency permittivity of biological tissues with an open-ended coaxial line: Part I," *IEEE Transactions on Microwave Theory and Techniques*, Vol. 30, No. 1, 82–86, 1982.

[33] Liu, L., D. Xu, and Z. Jiang, "Improvement in dielectric measurement technique of open-ended coaxial line resonator method," *Electronics Letters*, Vol. 22, No. 7, 373–375, 1986.

[34] Hagl, D. M., D. Popovic, S. C. Hagness, J. H. Booske, and M. Okoniewski, "Sensing volume of open-ended coaxial probes for dielectric characterization of breast tissue at microwave frequencies," *IEEE Transactions on Microwave Theory and Techniques*, Vol. 51, No. 4, 1194–1206, 2003.

[35] Zajíček, R., J. Vrba, and K. Novotný, "Evaluation of a reflection method on an open-ended coaxial line and its use in dielectric measurements," *Acta Polytechnica*, Vol. 46, No. 5, 50–54, 2006.

[36] Zajíček, R., L. Oppl, and J. Vrba, "Broadband measurement of complex permittivity using reflection method and coaxial probes," *Radioengineering*, Vol. 17, No. 1, 14–19, 2008.

[37] CST STUDIO SUITE 2014, Available: https://www.3ds.com/products-services/simulia/products/cst-studio-suite (accessed on 09-08-2021).

[38] Weiland, T., "A discretization method for the solution of Maxwell's equations for six-component fields," *Electronics and Communications AEU*, Vol. 31, No. 3, 116–120, 1977.

[39] Clemens, M. and T. Weiland, "Discrete electromagnetism with the finite integration technique," *Progress In Electromagnetics Research*, Vol. 32, 65–87, 2001.

[40] IEC/IEEE International Standard, "Determining the peak spatial-average specific absorption rate (SAR) in the human body from wireless communications devices, 30 MHz to 6 GHz — Part 1: General requirements for using the finite-difference time-domain (FDTD) method for SAR calculations," *IEC/IEEE 62704-1: 2017*, 1–86, United States, 2017.

[41] Stuchly, S. S., M. A. Stuchly, A. Kraszewski, and G. Hartsgrove, "Energy deposition in a model of man: Frequency effects," *IEEE Transactions on Biomedical Engineering*, Vol. 33, No. 7, 702–711, 1986.

[42] Meier, K., V. Hombach, R. Kastle, R. Y.-S. Tay, and N. Kuster, "The dependence of electromagnetic energy absorption upon human-head modeling at 1800 MHz," *IEEE Transactions on Microwave Theory and Techniques*, Vol. 45, No. 11, 2058–2062, 1997.

[43] Cooper, J., B. Marx, J. Buhl, and V. Hombach, "Determination of safety distance limits for a human near a cellular base station antenna, adopting the IEEE standard or ICNIRP guidelines," *Bioelectromagnetics*, Vol. 23, No. 6, 429–443, 2002.

[44] Christ, A., A. Klingenbock, T. Samaras, C. Goiceanu, and N. Kuster, "The dependence of electromagnetic far-field absorption on body tissue composition in the frequency range from 300 MHz to 6 GHz," *IEEE Transactions on Microwave Theory and Techniques*, Vol. 54, No. 5, 2188–2195, 2006.

[45] Karunarathna, M. A. A. and I. J. Dayawansa, "Energy absorption by the human body from RF and microwave emissions in Sri Lanka," *Sri Lankan Journal of Physics*, Vol. 7, 35–47, 2006.

[46] Yelkenci, T., "Effects of metallic objects on specific absorption rate in the human head for 915 and 1900 MHz mobile phones," *Frequenz*, Vol. 60, No. 3-4, 46–50, 2006.

[47] Yelkenci, T. and S. Paker, "The effects of frequency, polarization, direction and metallic objects on the SAR values in a human head model for plane wave exposure (500–2500 MHz)," *Frequenz*, Vol. 60, No. 11-12, 215–219, 2006.

[48] Hirata, A., N. Ito, O. Fujiwara, T. Nagaoka, and S. Watanabe, "Conservative estimation of whole-body-averaged SARs in infants with a homogeneous and simple-shaped phantom in the GHz region," *Physics in Medicine & Biology*, Vol. 53, No. 24, 7215–7223, 2008.

[49] Iyama, T., T. Onishi, Y. Tarusawa, S. Uebayashi, and T. Nojima, "Novel specific absorption rate (SAR) measurement method using a flat solid phantom," *IEEE Transactions on Electromagnetic Compatibility*, Vol. 50, No. 1, 43–51, 2008.

[50] Simba, A. Y., T. Hikage, S. Watanabe, and T. Nojima, "Specific absorption rates of anatomically realistic human models exposed to RF electromagnetic fields from mobile phones used in elevators," *IEEE Transactions on Microwave Theory and Techniques*, Vol. 57, No. 5, 1250–1259, 2009.

[51] Wessapan, T., S. Srisawatdhisukul, and P. Rattanadecho, "Specific absorption rate and temperature distributions in human head subjected to mobile phone radiation at different frequencies," *International Journal of Heat and Mass Transfer*, Vol. 55, No. 1-3, 347–359, 2012.

[52] Wessapan, T. and P. Rattanadecho, "Specific absorption rate and temperature increase in the human eye due to electromagnetic fields exposure at different frequencies," *International Journal of Heat and Mass Transfer*, Vol. 64, 426–435, 2013.

[53] Lin-Liu, S. and W. R. Adey, "Low frequency amplitude modulated microwave fields change calcium efflux rates from synaptosomes," *Bioelectromagnetics*, Vol. 3, No. 3, 309–322, 1982.

[54] Kwee, S. and P. Raskmark, "Changes in cell proliferation due to environmental non-ionizing radiation: 2. Microwave radiation," *Bioelectrochemistry and Bioenergetics*, Vol. 44, No. 2, 251–255, 1998.

[55] Velizarov, S., P. Raskmark, and S. Kwee, "The effects of radiofrequency fields on cell proliferation are non-thermal," *Bioelectrochemistry and Bioenergetics*, Vol. 48, No. 1, 177–180, 1999.

[56] Navarro, E. A., J. Segura, M. Portolés, and C. G. de Mateo, "The microwave syndrome: A preliminary study in Spain," *Electromagnetic Biology and Medicine*, Vol. 22, No. 2-3, 161–169, 2003.

[57] Remondini, D., R. Nylund, J. Reivinen, F. P. de Gannes, B. Veyret, I. Lagroye, E. Haro, M. A. Trillo, M. Capri, C. Franceschi, and K. Schlatterer, "Gene expression changes in human cells after exposure to mobile phone microwaves," *Proteomics*, Vol. 6, No. 17, 4745–4754, 2006.

[58] Hinrikus, H., M. Bachmann, D. Karai, and J. Lass, "Mechanism of low-level microwave radiation effect on nervous system," *Electromagnetic Biology and Medicine*, Vol. 36, No. 2, 202–212, 2017.

[59] Panagopoulos, D. J., M.-C. Cammaerts, D. Favre, and A. Balmori, "Comments on environmental impact of radiofrequency fields from mobile phone base stations," *Critical Reviews in Environmental Science and Technology*, Vol. 46, No. 9, 885–903, 2016.

[60] Panagopoulos, D. J., E. D. Chavdoula, and L. H. Margaritis, "Bioeffects of mobile telephony radiation in relation to its intensity or distance from the antenna," *International Journal of Radiation Biology*, Vol. 86, No. 5, 345–357, 2010.

[61] Sivani, S. and D. Sudarsanam, "Impacts of radio-frequency electromagnetic field (RF-EMF) from cell phone towers and wireless devices on biosystem and ecosystem — A review," *Biology and Medicine*, Vol. 4, No. 4, 202–216, 2012.

[62] Roux, D., A. Vian, S. Girard, P. Bonnet, F. Paladian, E. Davies, and G. G. Ledoigt, "Electromagnetic fields (900 MHz) evoke consistent molecular responses in tomato plants," *Physiologia Plantarum*, Vol. 128, No. 2, 283–288, 2006.

[63] Roux, D., C. Faure, P. Bonnet, S. Girard, G. Ledoigt, E. Davies, M. Gendraud, F. Paladian, and A. Vian, "A possible role for extra-cellular ATP in plant responses to high frequency, low amplitude electromagnetic field," *Plant Signaling & Behavior*,

Vol. 3, No. 6, 383–385, 2008.

[64] Kundu, A., S. Vangaru, S. Bhattacharyya, A. I. Mallick, and B. Gupta, "Electromagnetic irradiation evokes physiological and molecular alterations in rice," *Bioelectromagnetics*, Vol. 42, No. 2, 173–185, 2021.

[65] Kundu, A., S. Vangaru, S. Bhattacharyya, A. I. Mallick, and B. Gupta, "Erratum: Electromagnetic irradiation evokes physiological and molecular alterations in rice," *Bioelectromagnetics*, Vol. 42, No. 5, 435, 2021.

[66] Kundu, A., S. Vangaru, S. Bhowmick, S. Bhattacharyya, A. I. Mallick, and B. Gupta, "One-time electromagnetic irradiation modifies stress-sensitive gene expressions in rice plant," *Bioelectromagnetics*, Vol. 42, No. 8, 649–658, 2021.

[67] Kumar, G., "Report on cell tower radiation," 1-50, submitted to Secretary, Department of Telecommunications, India, 2010.

[68] Bhattacharya, K., "On the dependence of charge density on surface curvature of an isolated conductor," *Physica Scripta*, Vol. 91, No. 3, 035501, 2016.

[69] Jordan, E. C. and K. G. Balmain, *Electromagnetic Waves and Radiating Systems*, 2nd ed., PHI Learning, 2009.

[70] Deshpande, M. D., C. R. Cockrell, F. B. Beck, E. Vedeler, and M. B. Koch, "Analysis of electromagnetic scattering from irregularly shaped, thin, metallic flat plates," *NASA Technical Paper*, Article No. 3361, 1993.

[71] Kundu, A., "Investigations on the effects of electromagnetic radiation on Indian Flora," Ph.D. dissertation, Jadavpur University, India, 2022.

[72] Kundu, A., B. Gupta, and A. I. Mallick, "Dependence of specific absorption rate and its distribution inside a homogeneous fruit model on frequency, angle of incidence, and wave polarization," *Frequenz*, Vol. 76, No. 1-2, 109–119, 2022.

[73] Mukherjee, N., A. Kundu, and M. Mitra, "Study of SAR data and spatial distribution in a peace lily plant model under different electromagnetic exposure scenarios," *Progress In Electromagnetics Research C*, Vol. 136, 61–74, 2023.